*Original scientific paper*

# Fabrication and optimization of freeze-dried isoniazid-loaded poly-$\varepsilon$-caprolactone nanoparticles

Eknath Kole[1], Yuvraj Pawara[2], Atul Chaudhari[1], Aniruddha Chatterjee[3] and Jitendra Naik[1,*]

[1]*Department of Pharmaceutical Technology, University Institute of Chemical Technology, KBC North Maharashtra University, Jalgaon MS 425001, India*
[2]*R. C. Patel Institute of Pharmaceutical Education and Research, Shirpur, MS 425405, India*
[3]*Plastics Engineering Department, Plastindia International University, Vapi, Gujarat, India*
Corresponding Author: E-mail*: *jitunaik@gmail.com*

## Abstract

**Background**: Microfluidic nanoprecipitation followed by freeze-drying would yield uniformly sized, stable nanoparticles by preserving their physicochemical property without compromising therapeutic performance. The isoniazid (INH)-loaded poly-$\varepsilon$-caprolactone (PCL) nanoparticles could be developed using a microfluidic technique for the management of tuberculosis. **Experimental approach:** The INH-loaded nanoparticles were fabricated via a microreactor-assisted nanoprecipitation method and optimization using a design of experiments factorial design approach. The resulting INH-PCL nanoformulation was characterized for particle size, polydispersity index (PDI), zeta potential (surface charge), Fourier-transform infrared spectroscopy, differential scanning calorimetry, X-ray diffraction analysis and field emission scanning electron microscope. **Key results:** The optimized nanoparticles exhibited an average particle size (248.4 ± 5.372 nm) and high encapsulation efficiency (82.26 ± 4.36 %). Thermal and spectroscopic analyses confirmed the absence of drug-polymer interactions, ensuring formulation integrity; stability studies under accelerated conditions demonstrated negligible changes in particle size, PDI, and zeta potential over the period of 6 months, indicating robust colloidal stability. A scanning electron microscopy study revealed rod-shaped nanoparticles with smooth surfaces. Lyophilization (freeze-drying) enhanced long-term stability, yielding a readily re-dispersible powder (reconstitution index ~1.066). Following diffusion-controlled kinetics, in vitro drug release studies in phosphate buffer saline (pH 7.4) showed sustained drug release (92.45 % cumulative release over 48 h). **Conclusion:** Our results confirm that the INH-loaded PCL nanoformulation combines excellent stability, high drug-loading capacity, and sustained release, key attributes of effective tuberculosis therapy.

### Keywords

Lyophilization; nanoprecipitation; microreactor, sustained release; pulmonary tuberculosis

## Introduction

Tuberculosis (TB), a life-threatening respiratory infection caused by *Mycobacterium tuberculosis* (*Mtb*), continues to pose a significant global health burden. The World Health Organization's 2024 report documented 10.8 million new TB cases and 1.25 million fatalities in 2023, underscoring the urgent need for improved treatments [1-3]. The TB infection cycle begins when aerosolized *Mtb* bacilli from an active case are inhaled into the lungs of a new host. Upon reaching the alveoli, the bacteria are phagocytosed by

macrophages, ultimately leading to the development of characteristic granulomatous lesions where the host attempts to isolate the persistent mycobacteria [4]. The gradual breakdown of granuloma integrity can enable *Mtb* reactivation and spread, resulting in destructive cavitary lung lesions. Successful TB treatment must address two distinct bacterial populations: latent organisms within granulomas and actively dividing bacilli in cavities, highlighting the need for multifaceted therapeutic solutions [5]. Conventional TB treatment follows a two-phase protocol, beginning with a 2-month course of four first-line drugs (isoniazid, rifampicin, pyrazinamide, and ethambutol), followed by a 4-month maintenance phase with isoniazid and rifampicin [6]. The extended 4 to 6-month treatment course and substantial daily medication load frequently result in therapeutic challenges. These include decreased patient adherence caused by adverse effects and pharmacological interactions, which may contribute to unsuccessful treatment outcomes and the emergence of drug-resistant tuberculosis strains [7].

Several factors complicate tuberculosis treatment adherence, including the requirement for multi-drug regimens, significant treatment expenses, and undesirable medication effects. These challenges are exacerbated by the poor taste of many antitubercular formulations, creating particular difficulties for children and often resulting in skipped medications that may compromise treatment success [8,9]. Clinical studies indicate that over 10 % of tuberculosis patients undergoing conventional first-line treatment (including isoniazid therapy) terminate their regimens hastily due to medication-related complications, particularly peripheral nerve damage and liver toxicity [10,11]. Advances in pharmaceutical engineering have facilitated the design of innovative drug delivery platforms, including nanoparticle-based carriers, lipid vesicles, and polymeric microparticles [12-17]. These systems enable the controlled co-delivery of multiple therapeutic agents with prolonged release kinetics [18,19]. Engineered nanodelivery systems demonstrate superior drug-carrying capacity, programmable release kinetics, and precise tissue targeting while meeting stringent biocompatibility requirements for medical use [20,21].

The development of polymeric nanocarriers has introduced new possibilities for precision medicine. Their biodegradable composition capitalizes on physiological transport mechanisms, including vascular leakiness in diseased tissues, to enhance drug localization while sustaining therapeutic plasma levels through pro-longed circulation kinetics [22-24]. Among synthetic biodegradable polymers, poly-ε-caprolactone (PCL) stands out for drug delivery applications due to its unique pharmaceutical advantages. Its demonstrated safety profile, predictable degradation behaviour, and formulation flexibility make it ideal for nanoparticle development. Researchers particularly value PCL's hydrophobic nature and permeability characteristics for sustained drug delivery. Notably, its degradation yields 6-hydroxycaproic acid, a biologically benign byproduct that preserves local pH stability [25,26].

Implementing QbD principles in nanoparticle development allows for a comprehensive evaluation of critical quality attributes. Through design of experiments (DoE) methodologies, formulators can simulta-neously (i) determine essential process parameters, (ii) minimize required experimental runs, and (iii) assess multivariate factor relationships, significantly streamlining nanomedicine development [27]. This study introduced a novel approach by combining microreactor-assisted nanoprecipitation with freeze-drying to fabricate and optimize isoniazid (INH)-loaded PCL nanoparticles (NPs). This strategy leverages the precision of microreactors to achieve monodisperse NPs with high drug encapsulation efficiency (EE) while ensuring long-term stability through lyophilization critical advancement for clinical translation. This work aims to syste-matically develop and characterize freeze-dried INH-loaded PCL nanoparticles, optimizing key parameters like flow rate, polymer-drug ratio and surfactant concentration to enhance nanoparticle properties such as particle size, zeta potential, EE and drug release study. Microfluidic nanoprecipitation would yield uniformly sized, stable NPs, and freeze-drying will preserve their physicochemical integrity without compromising

therapeutic performance. This optimized platform could pave the way for scalable, efficient TB treatment with reduced systemic side effects. Comprehensive characterization confirmed optimal nanoparticle characteristics (size <188 nm, PDI <0.3, high EE). The lead formulation achieved sustained INH release, addressing key challenges in TB treatment.

**Materials and methods**

*Materials*

Isoniazid (INH) was generously provided by Lupin Ltd. (Chhatrapati Sambhajinagar, India), while poly($\varepsilon$-caprolactone) (PCL) and lactose were obtained from Sigma-Aldrich (USA). Poloxamer 188 (P-188) was purchased from BASF (Mumbai, India). Mannitol was obtained from Hi-Media, Mumbai. All solvents, including methanol, acetone, and glacial acetic acid, along with sodium chloride, potassium chloride, hydrochloric acid, and sodium hydroxide, were procured from Sisco Research Laboratories Pvt. Ltd. (Mumbai, India). Disodium hydrogen phosphate, potassium dihydrogen phosphate, and Tween 80 were purchased from Merck India. All chemicals and reagents used are of analytical grade purity.

*Preparation of nanoparticles*

The INH-loaded PCL nanoparticles were prepared using a microreactor-assisted nanoprecipitation technique. The fabrication involved the following steps: First, 100 mg of PCL was dissolved in acetone under sonication for 15 minutes (designated organic phase-Solution A), and Tween 80 was used as a stabilizer. Simultaneously, an aqueous phase (Solution B) containing 0.1 wt.% poloxamer 188 (copolymer; surfactant) was prepared. Separately, 50 mg of INH was dissolved in 5 mL of double-distilled water and subsequently added to Solution B dropwise using a syringe. Solutions A (organic phase) and B (aqueous phase) were each stirred separately under constant magnetic agitation (600 rpm, 30 min) and then filtered through a 0.45 μm PVDF membrane (BSB Pharma, Thane) for further use. The filtered solutions were subsequently processed through a microreactor system (Amar II, Equipment, Mumbai) connected to an infusion pump (Uni Labs), maintaining a constant flow rate of 0.24 mL/min. The resulting nanosuspension was collected from the microreactor outlet under continuous stirring (400 rpm) at ambient temperature [27,28]. The INH-encapsulated nanoparticles were purified by three cycles of centrifugation (10,000 rpm, 60 min, 4 °C). As a control, blank PCL nanoparticles were prepared following the identical protocol without drug incorporation. The resuspended INH-loaded PCL nanoparticle formulation underwent pre-freezing at -20 °C for 12 h before lyophilization in a vacuum freeze-dryer (Boyikang Laboratory Instruments Inc., China) over a 48 h cycle and during the lyophilization, mannitol was added as cryoprotectant. The lyophilized nanoparticles were collected as a free-flowing powder, transferred to amber glass vials, and stored in a desiccator containing anhydrous silica gel at 25 ± 2 °C until subsequent characterization studies.

*Experimental design*

The optimization of INH-loaded PCL nanoparticles or nanoformulation was investigated using a Box-Behnken experimental design, and three independent variables were evaluated at three levels [29]. Based on preliminary screening studies, two polymer concentration parameters ($X_1$, $X_2$) and stabilizer content ($X_3$) were chosen as critical formulation factors. We examined three levels for the independent variables: low, medium and high, as outlined in Table 1.

These variables were examined for their effects on three key nanoparticle characteristics: average particle size ($Y_1$), PDI ($Y_2$), and surface charge ($Y_3$). The fabricated INH-loaded PCL nanoparticles were considered concerning critical variables, including particle size, PDI, and surface charge. The experimental run, consisting

of 17 randomized test conditions with triplicate runs, was generated using Design Expert® software, (Stat-Ease Inc., USA, https://www.statease.com/software/design-expert/) (Table 2).

**Table 1**. Experimental design framework for nanoparticle optimization: Independent variables (factors) with operational ranges and dependent variables (responses) with constraints in the Box-Behnken response surface methodology (RSM)

| Input variables (independent variables) | | Levels | | |
|---|---|---|---|---|
| | | Low (-1) | Medium (0) | High (+1) |
| Numeric factors | $X_1$: Amount of PCL, mg | 6.5 | 13 | 52 |
| | $X_2$: Amount of poloxamer 188, mg | 5 | 10 | 20 |
| | $X_3$: Amount of Tween 80, % w/v (stabilizer) | 0.1 | 0.2 | 0.5 |
| Responses (dependent variables) | | Constraints | | |
| $Y_1$: Particle size, nm | | Minimum | | |
| $Y_2$: Polydispersity index | | Minimum | | |
| $Y_3$: Zeta potential, mV | | ± less than 30 | | |

The polynomial equations representing the main effects, interaction, and linear and two-factor interaction (2FI) effects of the independent formulation variables demonstrated significant impacts on the measured responses. Additionally, 3D surfaces and contour plots were used to visually illustrate the effects of the independent variables on the dependent responses. This methodology follows modern quality-focused development approaches in nanoparticle formulation, allowing efficient optimization with minimal experimental runs while ensuring reliable reproducibility. Recent nanocarrier development studies have shown that the selected experimental design has proven particularly effective for pharmaceutical process optimization [30-32].

**Table 2**. Response surface methodology (RSM) outcomes for INH-loaded PCL nanoparticles: Independent variables, experimental results of dependent variables.

| | Independent variables | | | Dependent variables | | |
|---|---|---|---|---|---|---|
| | Factor 1 ($X_1$) | Factor 2 ($X_2$) | Factor 3 ($X_3$) | Response 1 ($Y_1$) | Response 2 ($Y_2$) | Response 3 ($Y_3$) |
| 1 | 0 | 0 | 0 | 201.1 | 0.221 | -19.3 |
| 2 | 0 | 0 | 0 | 153.2 | 0.235 | -20.2 |
| 3 | 0 | -1 | 1 | 267 | 0.086 | -20.4 |
| 4 | 0 | 0 | 0 | 136.5 | 0.253 | -16.3 |
| 5 | 0 | 1 | -1 | 321.9 | 0.269 | -24.3 |
| 6 | -1 | 1 | 0 | 212.8 | 0.161 | -21.8 |
| 7 | -1 | 0 | -1 | 193.1 | 0.295 | -22.21 |
| 8 | 1 | -1 | 0 | 169.7 | 0.139 | -11.4 |
| 9 | 1 | 0 | -1 | 190.3 | 0.209 | -16.4 |
| 10 | 1 | 1 | 0 | 248.4 | 0.067 | -24.8 |
| 11 | -1 | 0 | 1 | 211.5 | 0.071 | -21.3 |
| 12 | 0 | 0 | 0 | 164.9 | 0.119 | -16.78 |
| 13 | 1 | 0 | 1 | 207.5 | 0.088 | -14.9 |
| 14 | -1 | -1 | 0 | 268.4 | 0.105 | -11.5 |
| 15 | 0 | 0 | 0 | 206.6 | 0.046 | -17.28 |
| 16 | 0 | -1 | -1 | 182.23 | 0.261 | -14.59 |
| 17 | 0 | 1 | 1 | 196.35 | 0.178 | -15.72 |

*Particle size, polydispersity index and surface charge*

The physicochemical characterization of INH-loaded PCL nanoparticles was performed using dynamic light scattering (Nano ZS 90 Zetasizer, Malvern Instruments Ltd., UK). Main parameters were measured, including hydrodynamic diameter, polydispersity index (PDI), and surface charge (zeta potential). For analysis, nanoparticle suspensions were diluted (0.1 mL nanosuspension in 2 mL deionized water) and loaded into disposable cuvettes. Measurements were conducted at 25 °C with a 173° backscatter angle, with each sample analysed for 120 seconds [33]. Triplicate measurements were reported as mean ± SD.

## Encapsulation efficiency and drug loading

The drug encapsulation efficiency of INH-loaded PCL nanoparticles was quantified using UV-Vis spectroscopy (UV-2600i, Shimadzu, Japan). The nanosuspension was centrifuged at 10,000 rpm for 60 min at 4 °C using a Thermo Scientific Sorvall ST 8R centrifuge to separate the free drug from the nanosuspension. The supernatant containing unentrapped drug was analysed at 262 nm, using a pre-established calibration curve ($R^2$ = 0.9933) [27]. EE, % and drug loading (DL, wt.%) were calculated using standard formulas, Equations (1) and (2), with all measurements performed in triplicate (*n*=3).

$$DL = \frac{\text{Weight of entraped INH}}{\text{Weight of nanoparticles}} 100 \tag{1}$$

$$EE = \frac{\text{Total INH added-unbound INH}}{\text{Total INH added}} 100 \tag{2}$$

## Particle morphology

The morphological characteristics of INH-loaded PCL nanoparticles were analysed using field emission scanning electron microscopy (FE-SEM; JSM-IT300LV, JEOL, Japan). Before imaging, samples were sputter-coated with a 10 nm gold layer (JCE-3000FC coating system, JEOL, Japan) for 50 s to ensure conductivity and imaged at 10 *kV* accelerating voltage in secondary electron detection mode[31,34].

## Redispersibility

The reconstitution properties of lyophilized INH-loaded PCL nanoparticles were evaluated by dispersing 2 mg of the freeze-dried powder in 2 mL of purified water (Milli-Q grade). The redispersed nanoparticles were subsequently characterized for particle size distribution and surface charge using the dynamic light scattering technique [27].

## Fourier transform infrared spectroscopy

Fourier-transform infrared spectroscopy (FT-IR) analysis was performed using a Spectrum Two spectrometer (PerkinElmer, USA) equipped with a universal ATR accessory (diamond/ZnSe crystal). Samples were analysed in their pure form by direct placement on the ATR crystal. Spectral data were collected in transmission mode with a 4 cm$^{-1}$ resolution, averaging 16 scans per measurement under continuous dry air purge [35]. The analysis covered the mid-infrared region (4000 to 400 cm$^{-1}$) for pure INH, PCL, Poloxamer 188, and the INH-loaded nanoparticle formulation.

## Differential scanning calorimetry

The thermal behaviour of pure INH, PCL, Poloxamer 188, and the INH-loaded nanoparticle powder formulations was analysed using a differential scanning calorimeter (DSC-7020, Hitachi High-Tech Corporation, Japan). Approximately 5 mg of each sample was placed in hermetically sealed aluminium crucibles and subjected to a heating program from 30 to 700 °C at 20 °C per minute, under a constant nitrogen atmosphere. The thermograms obtained were analysed using TA7000 software (Hitachi High-Tech Corporation, Japan) [36,37].

## X-ray diffraction study

The powdered sample's crystalline properties and physical state were investigated using an X-ray diffractometer (Bruker AXS D8 Focus) equipped with a Cu Kα radiation source (*λ* = 0.15406 nm). The instrument was set to an operating voltage of 40 kV and a current of 40 mA. Samples of pure INH, PCL, Poloxamer 188, and the INH-loaded nanoparticle formulation were prepared by evenly spreading the powder into plastic sample

holders and gently flattening the surface with a glass slide [38,39]. XRD scans were performed at ambient temperature, covering a $2\theta$ angular range from 5° to 60° with a step size of 0.02° and a scanning rate of 1° min$^{-1}$.

### *In vitro aerosolization study*

A Next Generation Impactor (NGI, Copley Scientific, UK) connected to a Rotahaler® (Cipla) assessed the aerodynamic properties of lyophilized INH-PCL nanoparticles. Exactly 50 mg of powder blended with lactose was loaded into size-3 capsules. Using a calibrated vacuum pump, the system operated at 60 L/min for 4 s. Upon actuation, particles are deposited across NGI stages (0.54-8.06 µm cutoff diameters). The gravimetric analysis determined emitted dose (ED), fine particle fraction (FPF ≤5 µm), mass median aerodynamic diameter (MMAD), and geometric standard deviation (GSD) [40]. Experiments were executed in triplicate ($n$ = 3) to confirm reproducibility.

### *In vitro drug release*

Pure NH and INH-loaded PCL nanoparticle release profiles were evaluated under sink conditions using a dialysis bag method (MWCO: 12-14 kDa, Sigma-Aldrich). Samples (2 mL containing 50 mg of drug or formulation) were sealed in dialysis bags and immersed in 900 mL of phosphate-buffered saline (PBS, pH 7.4) maintained at 37.5 ± 0.5 °C with continuous agitation (50 rpm). 5 mL aliquots were withdrawn and replaced at predetermined intervals with fresh PBS to preserve sink conditions [41,42]. The collected samples were filtered (0.2 µm PVDF syringe filters) to remove particulates, and the filtrates were analysed for INH concentration via UV-Vis spectrophotometry ($\lambda$ = 262 nm). All experiments were performed in triplicate ($n$ = 3), with mean values reported.

### *Stability study*

The stability of INH-PCL nanoparticles was evaluated over 6 months under storage conditions at 25 °C. Formulations in sealed amber vials were monitored monthly for particle size, PDI and zeta potential changes to assess physicochemical stability[43].

### *Statistical analysis*

Experimental results are presented as mean ± standard deviation (SD) from triplicate independent measurements. Statistical significance *(*p<0.05, **p<0.01, ***p<0.001)* was determined by one-way ANOVA using OriginPro 10.1 (OriginLab, https://www.originlab.com/).

## Results and discussion

This study focused on developing isoniazid-loaded poly(ε-caprolactone) nanoparticles for sustained drug release. The nanoparticles were thoroughly characterized, and a design of experiments methodology was employed to optimize formulation parameters, with particular emphasis on controlling particle size and maximizing drug encapsulation efficiency.

### *Optimization of nanoparticles*

BBD was used to determine the effect of the independent variable on the dependent variables. The concentration of polymers (PCL, Poloxamer 188) and stabilizer percentage (Tween 80) were selected as independent variables. The dependent variables were the particle size, PDI, and surface charge. The effect of an independent variable on the dependent variables was analysed by constructing polynomial equations and counterplots. The obtained polynomial Equations (3) to (5) for the responses particle size ($Y_1$), PDI ($Y_2$) and surface charge ($Y_3$) are as follows:

$$Y_1 = 172.46 - 8.7375X_1 + 11.515X_2 - 0.6475X_3 + 33.575X_1X_2 + -52.58X_2X_3 + 5.5475X_1^2 + \\ + 46.8175X_2^2 + 22.5925X_3^2 \tag{3}$$

$$Y_2 = 0.164882 - 0.016125X_1 + 0.0105X_2 - 0.076375X_3 \tag{4}$$

$$Y_3 = -18.1871 + 1.16375X_1 - 3.59125X_2 + 0.6475X_3 \tag{5}$$

As the above equations state, the positive sign indicates the independent variable's synergic effect, whereas a negative sign indicates the antagonistic effect. The polynomial equations and statistical analysis reveal a distinct relationship between the formulation variable and nanoparticle properties. Equation (3) (particle size) exhibited synergistic and antagonistic effects of the independent variables. The negative coefficient of $X_1$ (-8.7375) suggests an antagonistic effect, implying that increased PCL concentration reduces particle size. Conversely, $X_2$ concentration exhibited a synergistic effect, which increased particle size, while $X_3$ (-0.6475) had a mild antagonistic effect. A significant interaction was observed between the $X_1X_2$ (+33.575) and $X_2X_3$ (-52.58), indicating complex synergetic and antagonistic interdependencies. The optimized formulation (run 10) resulted in a minimal average particle size of 248.4±5.37 nm, highlighting the microreactor-assisted synthesis's efficiency. In Equation (4) (PDI), all three variables exhibited antagonistic or minimal effects. $X_1$ (-0.016125) and $X_3$ (-0.076375) contributed to a decrease in PDI, implying improved uniformity, while $X_2$ (+0.0105) slightly increased PDI. The optimized batch (run 10) demonstrated a PDI of 0.067±0.011, indicating narrow size distributions and good nanoparticle homogeneity. Equation (5) (surface charge) showed the synergetic effect of $X_1$ (+1.16375), increasing surface charge, whereas $X_2$ (-3.591250 exhibited an antagonistic effect, and $X_3$ (+0.6475) showed a mild synergetic impact. These effects reflect the electrostatic stability of nanoparticles, which is crucial for maintaining colloidal dispersion. The optimized batch (run 10) demonstrated a surface charge of -24.8 ± 0.30 mV, indicating acceptable colloidal stability of nanoparticles. The coefficient of determination ($R^2$) values for $Y_1$, $Y_2$, and $Y_3$ were 0.6633, 0.3455, and 0.3240, respectively. These values suggest a moderately good fit for the particle size model ($Y_1$) and lower predictive accuracy for PDI ($Y_2$) and surface charge ($Y_3$). Nonetheless, the p-values of 0.0281 ($Y_1$), 0.0368 ($Y_2$), and 0.0447 ($Y_3$) confirm the statistical significance of the models at the $p < 0.05$ level (Table 3).

**Table 3**. Statistical summary of the Box-Behnken design (BBD) model for optimization of INH-loaded PCL nanoparticles

| | Source | Sequential $p$-value | Lack of fit $p$-value | Adjusted $R^2$ | Predicted $R^2$ |
|---|---|---|---|---|---|
| Particle size | Linear | 0.8804 | 0.1199 | -0.1712 | -0.7151 |
| | Two-factor interaction | 0.0823 | 0.2021 | 0.1975 | -0.4263 |
| | Quadratic (suggested) | 0.0281 | 0.7024 | 0.6633 | 0.1901 |
| | Cubic (aliased) | 0.7024 | | 0.5714 | |
| PDI | Linear (suggested) | 0.0368 | 0.9126 | 0.3455 | 0.1786 |
| | Two-factor interaction | 0.6337 | 0.8827 | 0.2776 | -0.1068 |
| | Quadratic | 0.4683 | 0.9532 | 0.2658 | 0.1613 |
| | Cubic (aliased) | 0.9532 | | -0.1916 | |
| Zeta potential | Linear (suggested) | 0.0447 | 0.0653 | 0.3240 | -0.1066 |
| | Two-factor interaction | 0.1725 | 0.0831 | 0.4546 | -0.5720 |
| | Quadratic | 0.9293 | 0.0334 | 0.2666 | -3.5006 |
| | Cubic (aliased) | 0.0334 | | 0.8245 | |

Analysis of variance (ANOVA) results in Table 4 further validated model adequacy. The interaction terms were statistically significant, particularly for $Y_1$ ($p < 0.0015$), with an associated $F$-value of 0.4996. The $F$-values for $Y_2$ and $Y_3$ were 0.3489 and 5.12, respectively, indicating that the model terms contribute meaningfully to predicting response behaviour.

The 2D contour plots and 3D response surface diagrams (Figures 1A-1C**')** were generated to elucidate the relationships between variables.

**Table 4**. Summary of ANOVA for $Y_1$, $Y_2$, and $Y_3$ the response INH-loaded PCL nanoparticles

|  | Source | Degree of freedom | *F*-value | *p*-value |  |
|---|---|---|---|---|---|
| | Model | 9 | 4.50 | 0.0300 | Significant |
| | *A*: Amount of PCL | 1 | 0.8389 | 0.3902 | |
| | *B*: Amount of poloxamer 188 | 1 | 1.46 | 0.2666 | |
| | *C*: Amount of stabilizer | 1 | 0.0046 | 0.9478 | |
| | *AB* | 1 | 6.19 | 0.0417 | |
| Particle size (*Y₁*) | *AC* | 1 | 0.0005 | 0.9829 | |
| | *BC* | 1 | 15.19 | 0.0059 | |
| | *A²* | 1 | 0.1780 | 0.6858 | |
| | *B²* | 1 | 12.68 | 0.0092 | |
| | *C²* | 1 | 2.95 | 0.1295 | |
| | Lack of fit | 3 | 0.4996 | 0.7024 | Not significant |
| | Model | 3 | 3.82 | 0.0368 | Significant |
| | *A*: Amount of PCL | 1 | 0.4797 | 0.5007 | |
| PDI (*Y₂*) | *B*: Amount of poloxamer 188 | 1 | 0.2034 | 0.6594 | |
| | *C*: Amount of stabilizer | 1 | 10.76 | 0.0060 | |
| | Lack of fit | 9 | 0.3489 | 0.9126 | Not significant |
| | Model | 3 | 3.56 | 0.0447 | Significant |
| | *A*: Amount of PCL | 1 | 0.9848 | 0.3391 | |
| Zeta potential (*Y₃*) | *B*: Amount of poloxamer 188 | 1 | 9.38 | 0.0091 | |
| | *C*: Amount of stabilizer | 1 | 0.3049 | 0.5902 | |
| | Lack of Fit | 9 | 5.12 | 0.0653 | Not significant |
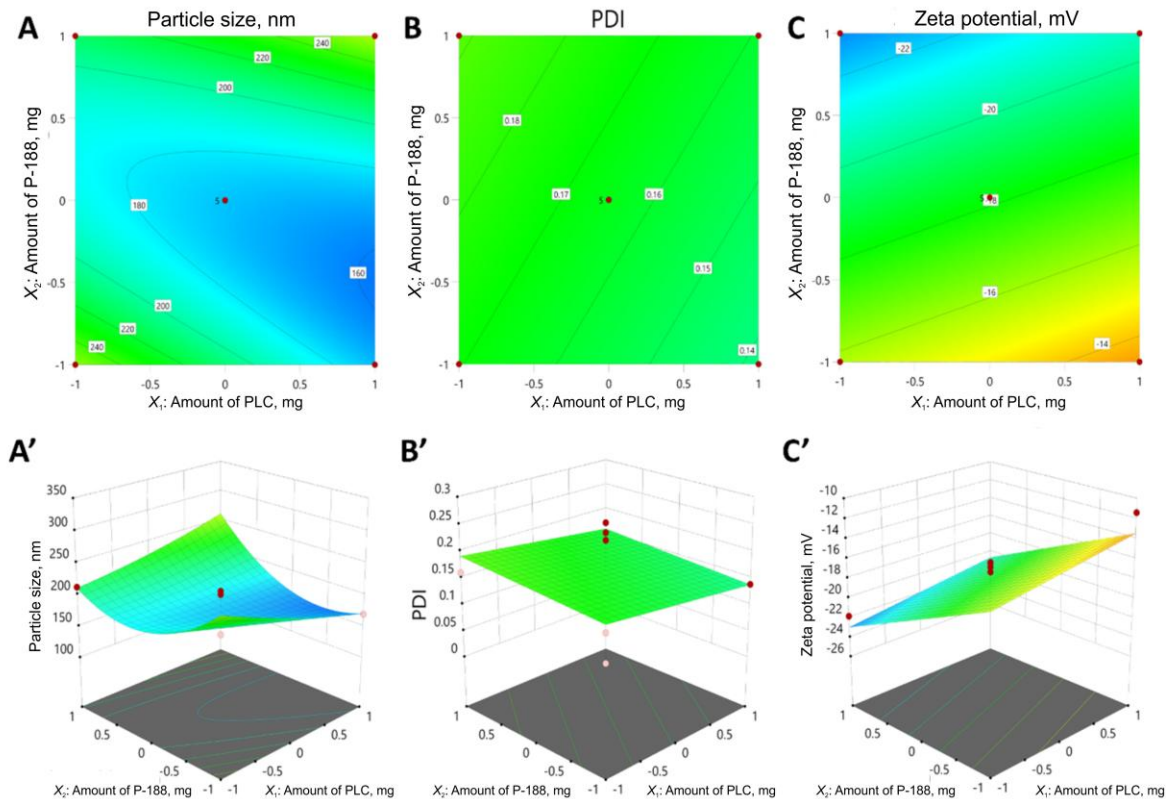


**Figure 1**. Response surface methodology (RSM) analysis of the Box-Behnken design: (A, A') 2D contour and 3D response surface plots illustrating the effect of independent variables on particle size; (B, B') polydispersity index (PDI); and (C, C') zeta potential

These graphs effectively map the influence of independent variables on the characteristics of INH-loaded PCL nanoparticles, which aids in identifying optimal experimental conditions while reinforcing the statistical findings.

## Particle size, PDI and zeta potential

The optimized INH-loaded PCL nanoformulation exhibited favourable physicochemical properties with a mean hydrodynamic diameter of 248.4±5.37 nm (Figure 2A), indicating successful nanoparticle formation. The narrow polydispersity index (0.067±0.011) confirmed a homogeneous size distribution, while the zeta potential of -24.8±0.30 mV (Figure 2B) suggested good colloidal stability. These results validate the effectiveness of the microreactor-assisted nanoprecipitation method for producing INH-loaded PCL nanoparticles with optimal characteristics.
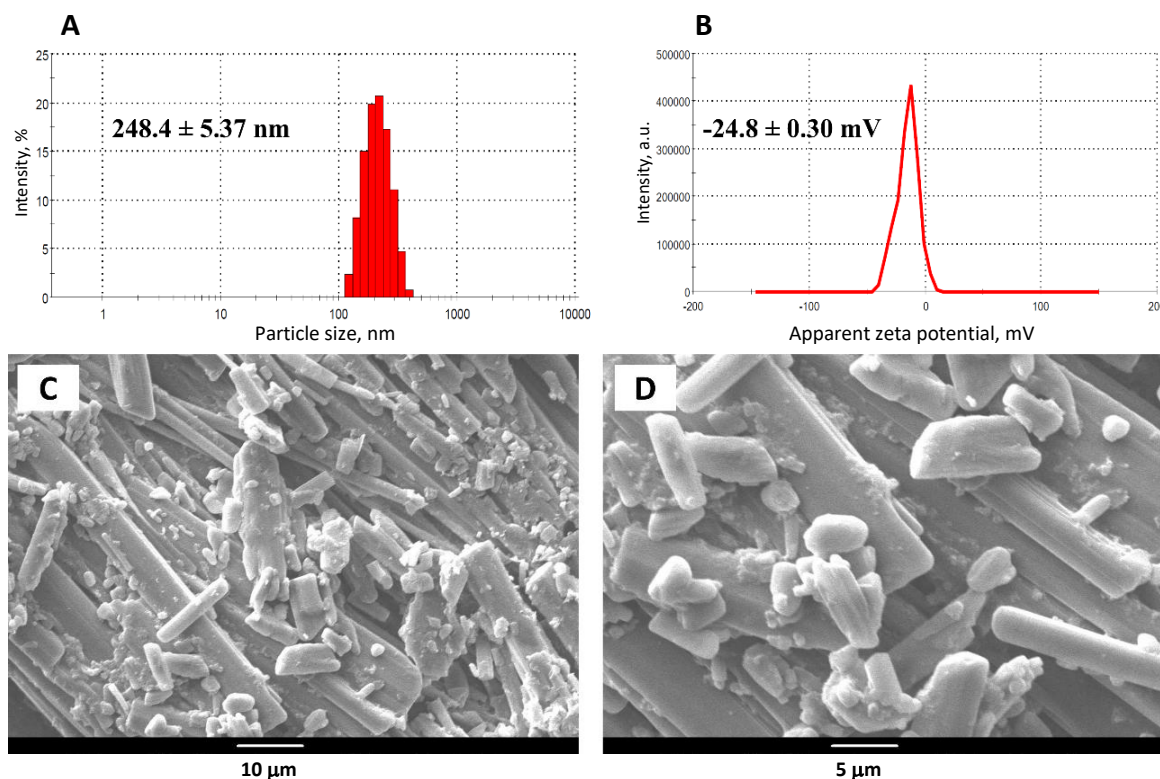


**Figure 2**. Physicochemical characterization of INH-loaded PCL nanoparticles: (A) hydrodynamic size distribution, (B) surface charge (zeta potential) (dynamic light scattering, DLS), Data represent mean ± *SD* (*n* = 3) and (C, D) scanning electron microscopy (SEM) micrographs (acceleration voltage: 10 kV)

## Entrapment efficiency and drug loading

The encapsulation efficiency of the lyophilized INH-loaded PCL nanoparticles was evaluated by analysing the supernatant. This involved quantifying the unencapsulated INH in the aqueous phase and comparing it to the initial theoretical drug input. The INH-loaded PCL nanoparticles exhibited high drug encapsulation efficiency (82.26±4.36 %) and a loading capacity of 9.28±0.28 wt.% (mean ± SD, *n* = 3). Several studies utilizing PCL-based nanoparticle systems have reported drug loading capacities and encapsulation efficiencies comparable to our results. Notably, Zhang *et al*. [44] research employing PCL/Poloxamer 188 nanoparticles achieved a loading capacity of 10.05 %, while plain PCL nanoparticles showed a slightly lower value of 9.98 %, with both systems demonstrating encapsulation efficiencies above 70 %. These findings corroborate our experimental outcomes and validate the effectiveness of PCL-based delivery systems for hydrophobic drug encapsulation [23,45]. These metrics confirm the successful entrapment of isoniazid within the polymeric matrix, highlighting the formulation's robust drug-loading capabilities.

## Particle morphology

The SEM images of lyophilized INH-loaded PCL nanoparticle formulation revealed a rod-like crystal structure with a smooth surface and smaller particles adhered, indicating agglomeration. Figure 2C-2D Freeze-drying led to particle clustering and possible crystallization, affecting overall nanoparticle morphology [27] .

*Redispersibility index*

The redispersion behaviour of lyophilized INH-loaded PCL nanoparticles was thoroughly investigated to evaluate formulation stability and reconstitution potential. The lyophilized INH-PCL nanoparticles exhibited excellent redispersibility, reforming stable nanoparticles (264.96±10.87 nm) with low polydispersity (0.129±0.037) and good colloidal stability (-19.7 ± 0.60 mV) upon reconstitution. The RDI (~1.066) confirmed ideal reconstitution with minimal aggregation. These results demonstrate the successful preservation of nanoscale properties during lyophilization. The formulation maintains pharmaceutical suitability post-freeze-drying and storage.

*Fourier transform infrared spectroscopy*

The FTIR spectrum of INH exhibited characteristic functional group peaks, including O-H stretching at 3239.82 cm$^{-1}$, N-H stretching at 3461.69 cm$^{-1}$, C≡N stretching at 2212.17 cm$^{-1}$, C=O stretching at 1716.35 cm$^{-1}$, CH$_3$ stretching at 1133.34 cm$^{-1}$, N-H bending at 1629.98 cm$^{-1}$, pyridine ring vibrations at 1403.65 cm$^{-1}$ and free NH$_2$ at 1215.17 cm$^{-1}$, confirming its structural integrity [46]. Similarly, PCL displayed distinct absorptions for asymmetric CH$_2$ stretching (2979.00 cm$^{-1}$), symmetric CH$_2$ stretching (2893.19 cm$^{-1}$), C=O stretching (1813.80 cm$^{-1}$), and asymmetric COC stretching (1717.89, 1667.28 and 1149.65 cm$^{-1}$), validating its polymer structure [47]. Poloxamer-188 showed prominent peaks for O-H stretching (3404.49 cm$^{-1}$), aliphatic C-H stretching (2881.09 cm$^{-1}$), in-plane O-H bending (1363.27 cm$^{-1}$), and C-O stretching (2117.85 cm$^{-1}$), consistent with reported data [48]. In the INH-loaded PCL nanoparticles, the spectrum revealed overlapping drug and polymer peaks with minor shifts: O-H stretching (3274.65 cm$^{-1}$), N-H stretching (3380.81 cm$^{-1}$), C≡N stretching (2201.84 cm$^{-1}$), C=O stretching (1664.07 cm$^{-1}$), CH$_3$ stretching (1191.58 cm$^{-1}$), N-H bending (1632.59 cm$^{-1}$), pyridine ring vibrations (1430.68 cm$^{-1}$), asymmetric CH$_2$ stretching (2932.89 cm$^{-1}$), symmetric CH$_2$ stretching (2880.72 cm$^{-1}$) and C-O/C-C stretching (1728.43 and 1664.07 cm$^{-1}$) (Figure 3A). The absence of new peaks or significant band shifts confirms that there is no chemical interaction between INH and excipients during nanoparticle fabrication.
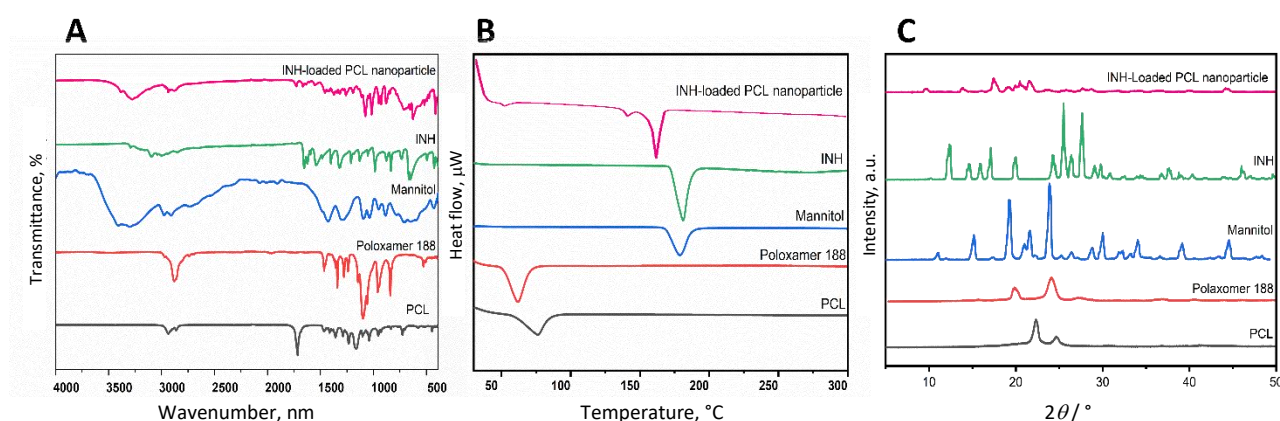


**Figure 3**. Solid-state analysis of INH-loaded PCL nanoparticles: (A) Fourier-transform infrared (FTIR) spectra, (B) differential scanning calorimetry (DSC) thermograms, and (C) X-ray diffraction (XRD) patterns

*Differential scanning calorimetry*

Figure 3B provides valuable information on the thermal behaviour and changes in the crystallinity of INH-loaded PCL nanoparticles compared to pure INH and individual excipients. Pure INH exhibited a distinct endothermic peak at 181.36 °C, corresponding to its melting point and indicating its crystalline structure. Similarly, mannitol exhibited a sharp peak at 178.40 °C, consistent with its known crystalline nature. Poloxamer-188, functioning as a surfactant, showed a mild endothermic transition around 61.44 °C, reflecting its semi-crystalline or low-crystallinity characteristics. PCL exhibited a melting peak at 75.79 °C, typical of semi-crystalline polymers. In contrast, the DSC thermogram of the INH-loaded PCL nanoparticles revealed notable differences.

The absence of the characteristic PCL melting peak indicates a disruption in the polymer's crystallinity, likely due to molecular-level interactions between INH and the PCL matrix during nanoparticle synthesis. This absence suggests that INH was successfully incorporated into the polymer network, forming an amorphous drug-polymer composite. Moreover, the melting point of INH shifted downward to 162.24 °C within the nanoparticles, suggesting a significant reduction in its crystallinity. Previously reported by Khuroo *et al*, [49] the development of rapid-dissolving printlets showed significant modification in the crystalline behaviour of INH. Their study observed the thermal behaviour of INH in the printlets formulation, which strongly supports the formation of an amorphous drug-polymer interaction or a reduction in crystallinity. This is evidenced by the shift in the INH melting peak from 174.8 °C (pure drug) to 168.3 to 168.9 °C (printlets), indicating disruption of the crystal lattice due to polymer interactions. This shift could be attributed to possible drug-polymer interactions or the formation of smaller and less stable crystalline domains of INH [49].

Additionally, a minor endothermic peak at 142.11 °C was observed, which may represent trace amounts of residual crystalline drug or interactions with excipients. However, the low intensity of this peak suggests a minimal impact on the overall system. Collectively, the DSC results demonstrate that INH was efficiently encapsulated within the PCL matrix, with notable changes in crystallinity supporting the formation of a well-integrated nanocarrier system optimized for drug delivery.

*X-ray diffraction analysis*

Figure 3C shows the XRD pattern of pure INH, PCL, Polaxomer-188 and INH-loaded PCL nanoparticles across the $2\theta$ range of 5 to 60˚. The XRD analysis revealed a distinct crystallinity pattern for each excipient: PCL showed characteristic peaks at 22.33 and 24.65˚, poloxamer 188 at 19.51 and 23.68˚, and mannitol exhibited multiple sharp peaks between 11.04 and 44.52˚, while pure INH demonstrated intense crystalline peaks from 12.37 to 46.08˚. The INH-loaded PCL nanoparticles displayed a modified diffraction pattern with peaks at 9.88, 17.60, 20.52 and 21.55˚, where the absence of Sharpe peaks and reduced PCL crystallinity indicates successful INH encapsulation and partial amorphization within the polymeric matrix. These structural changes, evidenced by peak broadening and shift, correlate with the formulation's sustained release behaviour of INH while maintaining sufficient nanoparticle stability through preserved PCL crystallinity. The XRD data collectively confirm the successful fabrication of polymeric nanoparticles for drug delivery with optimal physicochemical properties for sustained or controlled release.

*In-vitro aerosolization properties*

The aerosolization performance of INH-loaded PCL nanoparticles was evaluated using the NGI apparatus. The results of the deposition pattern demonstrated optimal particle distribution, with most drug depositions occurring below stage 3 (effective cutoff diameter <4.7 µm), indicating successful targeting of the bronchio-alveolar region where mycobacteria reside. Our developed formulation exhibited favourable aerodynamic characteristics, including a mass medium aerodynamic diameter (MMAD) of 4.9 µm, which falls within the ideal 1-5 µm range for efficient pulmonary delivery. Notably, the fine particle fractions (PFP) reached 40.1 %, confirming that a substantial proportion of particles were within the respirable size ranges (<5 µm). The high emitted dose of 92.4 % further demonstrated excellent powder dispersion from the delivery device. The narrow GSD (1.58) suggests consistent particle size distribution, while the MMAD and FPF demonstrate compatibility with deep lung delivery. The deposition profile, illustrated in Figure 4, provides compressive evidence of the formulation's suitability for inhalation therapy. The collective findings validate that the INH-loaded PCL nanoparticle formulations possess the necessary aerodynamic properties for effective deep lung depositions, making them promising candidates for targeted therapy against pulmonary tuberculosis.
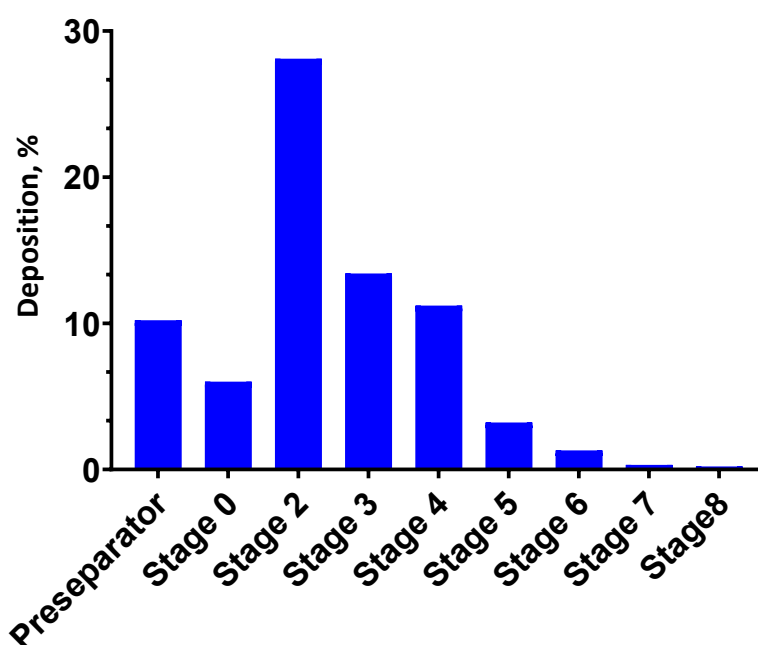
**Figure 4**. In vitro aerosolization behaviour of INH-loaded PCL nanoparticles

*In-vitro drug release study and kinetic study*

The *in vitro* drug release profiles of pure INH and INH-loaded PCL nanoparticles were evaluated using a dialysis method in PBS (pH 7.4). Pure INH exhibited a rapid release, with 96.66 % of the drug released within the first 2 h, indicating an immediate-release profile. In contrast, the INH-loaded PCL nanoformulation showed a sustained release pattern, with 21.50 % released at 2 h, 78.43 % at 24 h, and 92.45 % over 48 h. This extended-release behaviour highlights the controlled release capability of the PCL nanoparticle matrix, which can help maintain therapeutic drug levels over a prolonged period. Such a release profile offers significant therapeutic advantages, including reduced dosing frequency and improved patient compliance compared to conventional formulations. (Figure 5A) The drug release behaviour of INH-loaded PCL nanoparticles was analysed using various kinetic models, including zero-order, first-order, Higuchi, Hixson-Crowell, and Korsmeyer-Peppas models. (Figures 5B-5F) Among these, the first-order model exhibited the highest correlation coefficient ($R^2$ = 0.9750), indicating that the release rate depends on the remaining drug concentration and follows a concentration-gradient-driven mechanism. The zero-order ($R^2$ = 0.911) and Hixson-Crowell ($R^2$ = 0.9587) models also showed good fits, suggesting a controlled release profile possibly influenced by surface area reduction and matrix erosion. The Higuchi model ($R^2$ = 0.9259) revealed diffusion-based release through the polymer matrix (Table 5). The kinetic constant ($k$) was determined to be 3.9548, while the release exponent ($n$) of the Korsmeyer-Peppas equation was found to be 6.6785. The high value of the release exponents ($n$ >0.89) indicates that Super Case II transport (non-Fickian diffusion) governs the drug release. These findings strongly suggest that the dominant release mechanism involves substantial polymer relaxation and matrix swelling effects, rather than simple diffusion-controlled release [45].

**Table 5**. Release kinetic models of INH-loaded PCL nanoparticles

| Model | INH-loaded PCL nanoparticles | | |
| --- | --- | --- | --- |
| | $R^2$ | $k$ | $n$ |
| Zero order | 0.9110 | 3.9548 | 5.7665 |
| First order | 0.9750 | 0.0295 | 1.9967 |
| Higuchi model | 0.9259 | 18.046 | 8.2321 |
| Hixson-Crowell model | 0.9587 | 0.0869 | 0.0476 |
| Korsmeyer-peppas model | 0.9630 | 58.395 | 6.6785 |

Overall, the findings indicate that INH release from the nanoparticles is primarily governed by first-order kinetics, with additional contributions from diffusion and polymer degradation processes, supporting its potential for sustained drug delivery.
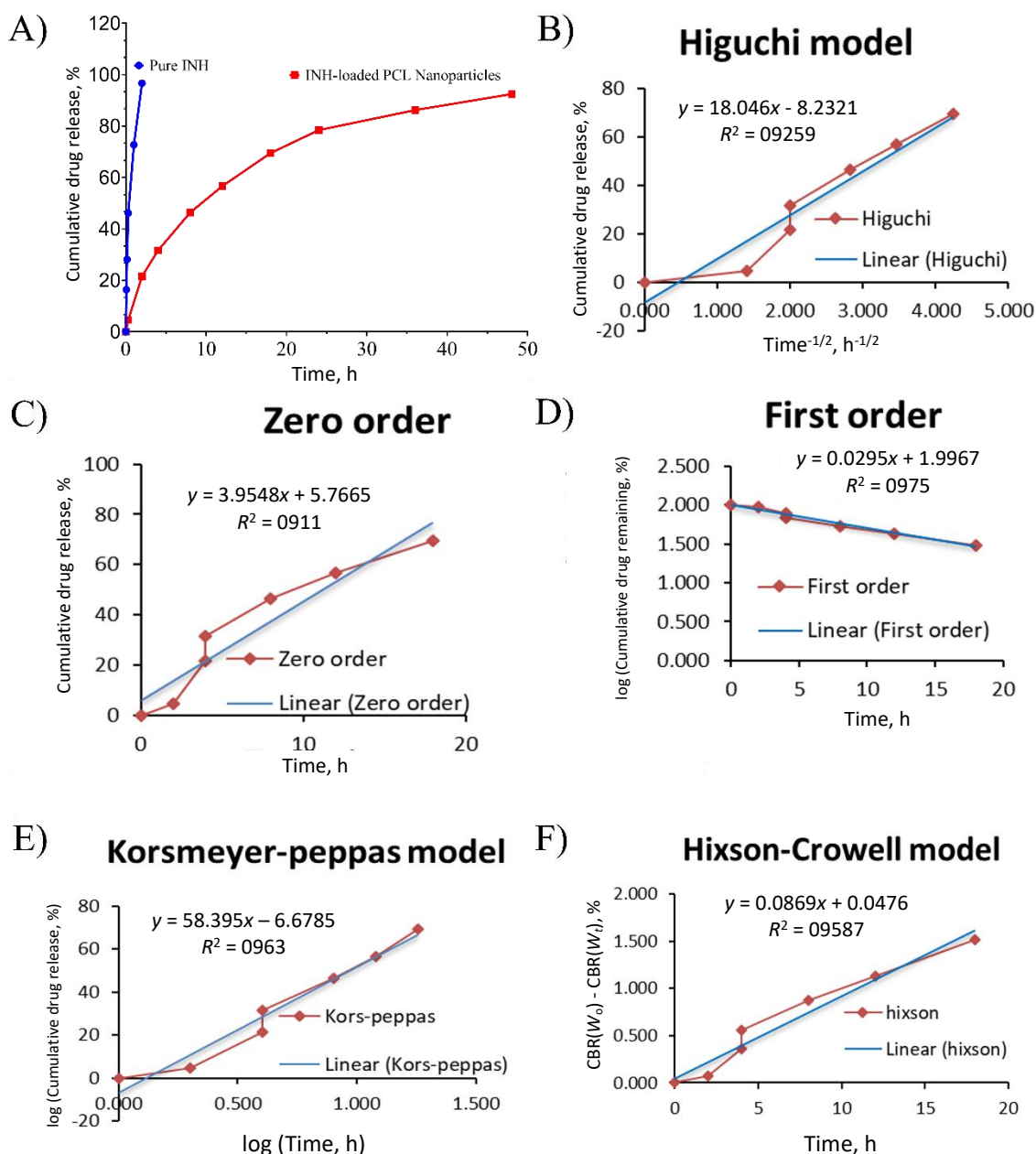


**Figure 5**. *In vitro* drug release and kinetic study. (A) cumulative release of pure INH and INH-loaded PCL nanoparticles ($n$ = 3; mean ± SD). Release kinetics fitted to (B) Higuchi, (C) zero-order, (D) first-order, (E) Korsmeyer-Peppas and (F) Hixson-Crowell models. (CBR - cumulative burst release, $W_o$ - initial weight, and $W_t$ - weight at time)

*Stability study*

The long-term stability of lyophilized INH-loaded PCL nanoparticles was evaluated under controlled storage conditions (25±2 °C) for six months. Throughout the study period, key physicochemical properties, such as particle size, zeta potential, and PDI, remained within acceptable ranges ($p > 0.05$), indicating no significant variations. The formulation also maintained its structural integrity, with no visible changes observed in its appearance. These findings demonstrate that the nanoformulation remains stable under ambient storage conditions (Figure 6A and B).
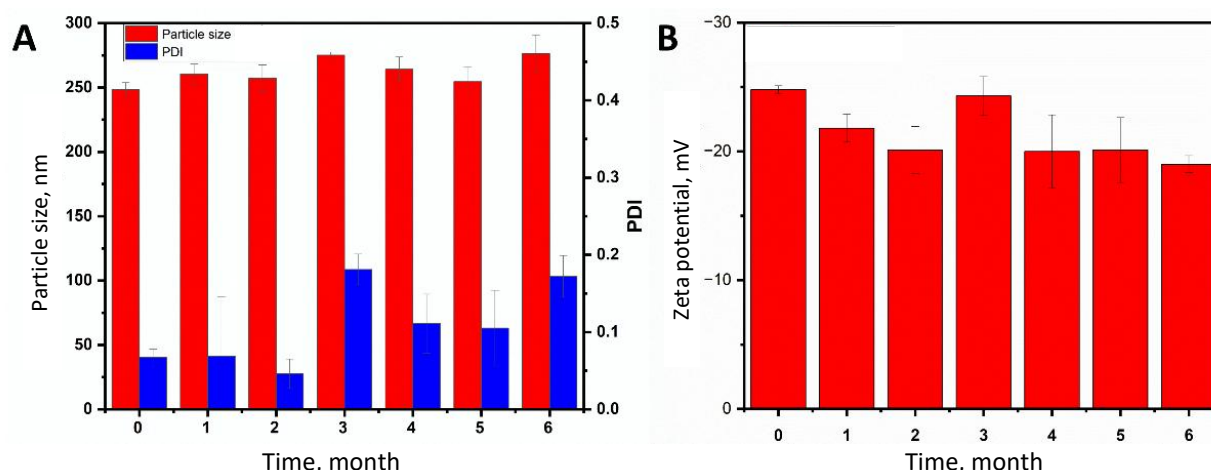
**Figure 6**. Stability evaluation of INH-loaded PCL nanoparticles stored under controlled conditions for six months:
(A) changes in particle size and polydispersity index and (B) zeta potential (mean±SD, *n*=3).

## Conclusions

In this study, we successfully developed freeze-dried isoniazid (INH)-loaded PCL nanoparticles using a micro-reactor-assisted nanoprecipitation method optimized through a BBD. The optimized formulation exhibited a uniform particle size of 248.4±5.372 nm, high drug encapsulation efficiency (82.26±4.36 %), and excellent colloidal stability under accelerated storage conditions over six months. Comprehensive physicochemical characterization (FTIR, DSC, XRD) confirmed the absence of drug-polymer interactions, while SEM analysis revealed a rod-like crystal structure and smooth-surfaced nanoparticles. In vitro release studies showed sustained, diffusion-controlled drug release, with 92.45 % cumulative release over 48 h. This INH-loaded PCL nanoformulation effectively addresses key challenges in tuberculosis therapy by combining high drug-loading capacity, prolonged release, and robust stability, offering a promising strategy to reduce dosing frequency and enhance patient compliance in pulmonary TB treatment. Future studies will focus on in vivo pharmacokinetic and biodistribution assessments to further evaluate the formulation's therapeutic potential and lung-targeting efficiency.

*Conflict of interest*: *The authors state that they have no competing financial interests or personal relationships that could have influenced the work presented in this paper.*

*Author Contributions:* *Eknath Kole: Conceptualization, Experimentation, Data Curation, Writing - Original Draft, Writing - Review & Editing, Yuvraj Pawara: Experimentation, Atul Chaudhari: Experimentation, Anniruddha Chatterjee: Writing - Review & Editing, Jitendra Naik: Writing - Review & Editing, Project Administration, Funding Acquisition, Supervision.*

*Data availability:* *The datasets generated during and/or analysed during the current study are not publicly available for technical reasons but are available from the corresponding author on reasonable request.*

## References

[1]    A.Z. Bahlool, B. Cavanagh, A.O. Sullivan, R. MacLoughlin, J. Keane, M.P.O. Sullivan, S.A. Cryan. Microfluidics produced ATRA-loaded PLGA NPs reduced tuberculosis burden in alveolar epithelial cells and enabled high delivered dose under simulated human breathing pattern in 3D printed head models. *European Journal of Pharmaceutical Sciences* **196** (2024) 106734. https://doi.org/10.1016/j.ejps.2024.106734

[2]    K.M.S.R. Sefat, M. Kumar, S. Kehl, R. Kulkarni, A. Leekha, M.M. Paniagua, D.F. Ackart, N. Jones, C. Spencer, B.K. Podell, H. Ouellet, N. Varadarajan. An intranasal nanoparticle vaccine elicits protective immunity against Mycobacterium tuberculosis. *Vaccine* **42(22)** (2024) 125909. https://doi.org/10.1016/j.vaccine.2024.04.055

[3]    Global tuberculosis report 2024. Geneva: World Health Organization, 2024. ISBN 978-92-4-010153-1

[4]    L. Luies, I. du Preez. The Echo of Pulmonary Tuberculosis: Mechanisms of Clinical Symptoms and Other Disease-Induced Systemic Complications. *Clinical Microbiology Reviews* **33(4)** (2020) 10-1128. https://doi.org/10.1128/CMR.00036-20

[5]    C.B.E. Chee, R. Reves, Y. Zhang, R. Belknap. Latent tuberculosis infection: Opportunities and challenges. *Respirology* **23** (2018) 893-900. https://doi.org/10.1111/resp.13346

[6]    A. Mobed, V. Alivirdiloo, S. Gholami, A. Moshari, A. Mousavizade, R. Naderian, F. Ghazi. Nano-Medicine for Treatment of Tuberculosis, Promising Approaches Against Antimicrobial Resistance. *Current Microbiology* **81** (2024) 326. https://doi.org/10.1007/s00284-024-03853-z

[7]    S.M. Patil, A.M. Diorio, P. Kommarajula, N.K. Kunda. A quality-by-design strategic approach for the development of bedaquiline-pretomanid nanoparticles as inhalable dry powders for TB treatment. *International Journal of Pharmaceutics* **653** (2024) 123920. https://doi.org/10.1016/j.ijpharm.2024.123920

[8]    G. Fekadu, F. Bekele, K. Bekele, T. Girma, G. Mosisa, M. Gebre, T. Alemu, T. Tekle, B. Gamachu, A. Diriba. Adherence to Anti-Tuberculosis Treatment Among Pediatric Patients at Nekemte Specialized Hospital, Western Ethiopia. *Patient Preference and Adherence* **14** (2020) 1259-1265. https://doi.org/10.2147/ppa.s258292

[9]    S. Bea, H. Lee, J.H. Kim, S.H. Jang, H. Son, J.-W. Kwon, J.-Y. Shin. Adherence and Associated Factors of Treatment Regimen in Drug-Susceptible Tuberculosis Patients. *Frontiers in Pharmacology* **12** (2021) 625078. https://doi.org/10.3389/fphar.2021.625078

[10]    U.A. Boelsterli, K.K. Lee. Mechanisms of isoniazid-induced idiosyncratic liver injury: Emerging role of mitochondrial stress. *Journal of Gastroenterology and Hepatology* **29** (2014) 678-687. https://doi.org/10.1111/jgh.12516

[11]    T. Schaberg, K. Rebhan, H. Lode. Risk factors for side-effects of isoniazid, rifampin and pyrazinamide in patients hospitalized for pulmonary tuberculosis. *European Respiratory Journal* **9** (1996) 2026-2030. https://doi.org/10.1080/07373937.2024.2437691

[12]    K. Jadhav, E. Kole, A. Abhang, S. Rojekar, V. Sugandhi, R.K. Verma, A. Mujumdar, J. Naik. Revealing the potential of nano spray drying for effective delivery of pharmaceuticals and biologicals. *Drying Technology* (2024) 90-113. https://doi.org/10.1080/07373937.2024.2437691

[13]    S.R. Pardeshi, E.B. Kole, H.S. Kapare, S.M. Chandankar, P.J. Shinde, G.S. Boisa, S.S. Salgaonkar, P.S. Giram, M.P. More, P. Kolimi, D. Nyavanandi, S. Dyawanapelly, V. Junnuthula. Progress on Thin Film Freezing Technology for Dry Powder Inhalation Formulations. *Pharmaceutics* **14** (2022) 2632. https://doi.org/10.3390/pharmaceutics14122632

[14]    E. Kole, K. Jadhav, N. Shirsath, P. Dudhe, R.K. Verma, A. Chatterjee, J. Naik. Nanotherapeutics for pulmonary drug delivery: An emerging approach to overcome respiratory diseases. *Journal of Drug Delivery Science and Technology* **81** (2023) 104261. https://doi.org/10.1016/j.jddst.2023.104261

[15]    K. Jadhav, E. Kole, R. Singh, S.K. Rout, R.K. Verma, A. Chatterjee, A. Mujumdar, J. Naik. A critical review on developments in drying technologies for enhanced stability and bioavailability of pharmaceuticals. *Drying Technology* **42** (2024) 1415-1441. https://doi.org/10.1080/07373937.2024.2357181

[16]    E. Kole, K. Jadhav, Y. Sonar, M. Kapse, S.A. Patil, A. Kumar. Advances in spray drying technology for anti-tubercular formulation development : A comprehensive review. *Drying Technology* **43(1-2)** (2025) 53-89. https://doi.org/10.1080/07373937.2024.2437690

[17]    V. Jadhav, A. Roy, K. Kaur, A. Roy, K. Sharma, R. Verma, S. Rustagi, S. Malik. Current advancements in functional nanomaterials for drug delivery systems. *Nano-Structures & Nano-Objects* **38** (2024) 101177. https://doi.org/10.1016/j.nanoso.2024.101177

[18] G. Wyszogrodzka-Gaweł, P. Dorożyński, S. Giovagnoli, W. Strzempek, E. Pesta, W.P. Węglarz, B. Gil, E. Menaszek, P. Kulinowski. An Inhalable Theranostic System for Local Tuberculosis Treatment Containing an Isoniazid Loaded Metal Organic Framework Fe-MIL-101-NH$_2$—From Raw MOF to Drug Delivery System. *Pharmaceutics* **11** (2019) 687. https://doi.org/10.3390/pharmaceutics11120687

[19] L.C. Luciani-Giacobbe, A.M. Lorenzutti, N.J. Litterio, M.V. Ramírez-Rigo, M.E. Olivera. Anti-tuberculosis site-specific oral delivery system that enhances rifampicin bioavailability in a fixed-dose combination with isoniazid. *Drug Delivery and Translational Research* **11** (2021) 894-908. https://doi.org/10.1007/s13346-020-00847-9

[20] J.K. Patra, G. Das, L.F. Fraceto, E.V.R. Campos, M. del P. Rodriguez-Torres, L.S. Acosta-Torres, L.A. Diaz-Torres, R. Grillo, M.K. Swamy, S. Sharma, S. Habtemariam, H.-S. Shin. Nano based drug delivery systems: recent developments and future prospects. *Journal of Nanobiotechnology* **16** (2018) 71. https://doi.org/10.1186/s12951-018-0392-8

[21] M. Kumar, T. Virmani, G. Kumar, R. Deshmukh, A. Sharma, S. Duarte, P. Brandão, P. Fonte. Nanocarriers in Tuberculosis Treatment: Challenges and Delivery Strategies. *Pharmaceuticals* **16** (2023) 1360. https://doi.org/10.3390/ph16101360

[22] B. Begines, T. Ortiz, M. Pérez-Aranda, G. Martínez, M. Merinero, F. Argüelles-Arias, A. Alcudia. Polymeric Nanoparticles for Drug Delivery: Recent Developments and Future Prospects. *Nanomaterials* **10** (2020) 1403. https://doi.org/10.3390/nano10071403

[23] L. Eltaib. Polymeric Nanoparticles in Targeted Drug Delivery: Unveiling the Impact of Polymer Characterization and Fabrication. *Polymers* **17** (2025) 833. https://doi.org/10.3390/polym17070833

[24] R. Rajput, J. Narkhede, J.B. Naik. Nanogels as nanocarriers for drug delivery: A review. *ADMET and DMPK* **8** (2020) 1-15. https://doi.org/10.5599/admet.724

[25] O. Opriş, C. Mormile, I. Lung, A. Stegarescu, M.-L. Soran, A. Soran. An Overview of Biopolymers for Drug Delivery Applications. *Applied Sciences* **14** (2024) 1383. https://doi.org/10.3390/app14041383

[26] T.-H. Tsung, Y.-C. Tsai, H.-P. Lee, Y.-H. Chen, D.-W. Lu. Biodegradable Polymer-Based Drug-Delivery Systems for Ocular Diseases. *International Journal of Molecular Sciences* **24** (2023) 12976. https://doi.org/10.3390/ijms241612976

[27] E. Kole, K. Jadhav, Z. Khan, R.K. Verma, A. Chatterjee, A. Mujumdar, J. Naik. Engineered vildagliptin-loaded polymeric nanoparticles via microfluidic and spray drying for enhanced antidiabetic activity. *Future Journal of Pharmaceutical Sciences* **10** (2024) 156. https://doi.org/10.1186/s43094-024-00736-9

[28] A. Patil, S. Pardeshi, M. Kapase, P. Patil, M. More, S. Dhole, E. Kole, P. Deshmukh, A. Gholap, A. Mujumdar, J. Naik. Continuous preparation of sustained release vildagliptin nanoparticles using tubular microreactor approach. *Drying Technology* **42(4)** (2024) 661-673. https://doi.org/10.1080/07373937.2023.2298778

[29] S. Rohilla, R. Awasthi, A. Rohilla, S.K. Singh, D.K. Chellappan, K. Dua, H. Dureja. Optimizing gefitinib nanoliposomes by Box-Behnken design and coating with chitosan: A sequential approach for enhanced drug delivery. *ADMET and DMPK* **12(4)** (2024) 657-677. https://doi.org/10.5599/admet.2366

[30] A.A. Abdelbary, M.H.H. AbouGhaly. Design and optimization of topical methotrexate loaded niosomes for enhanced management of psoriasis: Application of Box-Behnken design, in-vitro evaluation and in-vivo skin deposition study. *International Journal of Pharmaceutics* **485** (2015) 235-243. https://doi.org/10.1016/j.ijpharm.2015.03.020

[31] Kole, E., Sonar, Y., Sarode, R. J., Chaudhari, A., & Naik, J. (2025). Development and characterisation of lyophilised ethambutol-loaded polymeric nanoparticles. *Journal of Applied Pharmaceutical Research* **13(2)** 172-180. https://doi.org/10.69857/joapr.v13i2.1093

[32] J.B. Naik, R.K. Deshmukh. Study of Formulation Variables Influencing Polymeric Microparticles by Experimental Design. *ADMET & DMPK* **2(1)** (2014) 63-70. https://doi.org/10.5599/admet.2.1.29

[33] P. Guo, B.A. Buttaro, H.Y. Xue, N.T. Tran, H.L. Wong. Lipid-polymer hybrid nanoparticles carrying linezolid improve treatment of methicillin-resistant Staphylococcus aureus (MRSA) harbored inside

bone cells and biofilms. *European Journal of Pharmaceutics and Biopharmaceutics* **151** (2020) 189-198. https://doi.org/10.1016/j.ejpb.2020.04.010

[34]    L. Patil, U. Verma, R. Rajput, P. Patil, A. Chaterjee, J.B. Naik. Development of olanzapine solid dispersion by spray drying technique using screening design for solubility enhancement. *ADMET and DMPK* **11** (2023) 615-627. https://doi.org/10.5599/admet.1998

[35]    G. Khairnar, V. Mokale, R. Khairnar, A. Mujumdar, J. Naik. Production of antihyerglycemic and antihypertensive drug loaded sustained release nanoparticles using spray drying technique: Optimization by Placket Burman Design. *Drying Technology* **40** (2022) 626-637. https://doi.org/10.1080/07373937.2020.1825292

[36]    A. Patil, S. Pardeshi, M. Kapase, P. Patil, M. More, S. Dhole, E. Kole, P. Deshmukh, A. Gholap, A. Mujumdar, J. Naik. Continuous preparation of sustained release vildagliptin nanoparticles using tubular microreactor approach. *Drying Technology* **42** (2024) 661-673. https://doi.org/10.1080/07373937.2023.2298778

[37]    B. Subaşı-Zarbaliyev, G. Kutlu, F. Törnük. Polyvinyl alcohol nanoparticles loaded with propolis extract: Fabrication, characterization and antimicrobial activity. *ADMET and DMPK* **11(4)** (2023) 587-600. https://doi.org/10.5599/admet.1740

[38]    S. Mandpe, E. Kole, V. Parate, A. Chatterjee, A. Mujumdar, J. Naik. Design, development, and evaluation of spray dried flurbiprofen loaded sustained release polymeric nanoparticles using QBD approach to manage inflammation. *Drying Technology* **41** (15) (2023) 1-13. https://doi.org/10.1080/07373937.2023.2251572

[39]    S. Mandpe, E. Kole, V. Parate, A. Chatterjee, A. Mujumdar, J. Naik. Development, QbD-based optimisation, in-vivo pharmacokinetics, and ex-vivo evaluation of Eudragit ® RS 100 loaded flurbiprofen nanoparticles for oral drug delivery. *Journal of Microencapsulation* **42(1)** (2024) 1-13. https://doi.org/10.1080/02652048.2024.2427294

[40]    K. Jadhav, A. Jhilta, R. Singh, E. Ray, N. Sharma, R. Shukla, A.K. Singh, R.K. Verma. Clofazimine nanoclusters show high efficacy in experimental TB with amelioration in paradoxical lung inflammation. *Biomaterials Advances* **154** (2023) 213594. https://doi.org/10.1016/j.bioadv.2023.213594

[41]    Y. Jiang, Y. Zhou, C.Y. Zhang, T. Fang. Co-delivery of paclitaxel and doxorubicin by ph-responsive prodrug micelles for cancer therapy. *International Journal of Nanomedicine* **15** (2020) 3319-3331. https://doi.org/10.2147/ijn.s249144

[42]    U. Verma, A. Mujumdar, J. Naik. Preparation of Efavirenz resinate by spray drying using response surface methodology and its physicochemical characterization for taste masking. *Drying Technology* **38** (2020) 793-805. https://doi.org/10.1080/07373937.2019.1590845

[43]    P. Wagh, A. Mujumdar, J.B. Naik. Preparation and characterization of ketorolac tromethamine-loaded ethyl cellulose micro-/nanospheres using different techniques. *Particulate Science and Technology* **37** (2019) 347-357. https://doi.org/10.1080/02726351.2017.1383330

[44]    Y. Zhang, L. Tang, L. Sun, J. Bao, C. Song, L. Huang, K. Liu, Y. Tian, G. Tian, Z. Li, H. Sun, L. Mei. A novel paclitaxel-loaded poly(ε-caprolactone)/Poloxamer 188 blend nanoparticle overcoming multidrug resistance for cancer treatment. *Acta Biomaterialia* **6** (2010) 2045-2052. https://doi.org/10.1016/j.actbio.2009.11.035

[45]    S.Y. Lipaikin, A.S. Dorokhin, G.A. Ryltseva, A. V. Oberenko, A. V. Shabanov, T.G. Volova, E.I. Shishatskaya. Investigation of drug release kinetics from biodegradable polyhydroxyalkanoate microparticles. *Reaction Kinetics, Mechanisms and Catalysis* (2025). https://doi.org/10.1007/s11144-025-02852-w

[46]    J.M. da S. Leite, L.M. de Santana, D. Nadvorny, B.O. de Abreu, J. de S. Rebouças, F.R. Formiga, M.F. de L.R. Soares, J.L. Soares-Sobrinho. Nanoparticle design for hydrophilic drugs: Isoniazid biopolymeric nanostructure. *Journal of Drug Delivery Science and Technology* **87** (2023) 104754 https://doi.org/10.1016/j.jddst.2023.104754

[47]    B. Mollaghadimi. Preparation and characterisation of polycaprolactone-fibroin nanofibrous scaffolds containing allicin. *IET Nanobiotechnology* **16** (2022) 239-249. https://doi.org/10.1049/nbt2.12092

[48]    X. Lin, Y. Shi, S. Yu, S. Li, W. Li, M. Li, S. Chen, Y. Wang, M. Cong. Preparation of Poloxamer188-b-PCL and Study on in vitro Radioprotection Activity of Curcumin-Loaded Nanoparticles. *Frontiers in Chemistry* **8** (2020) 212. https://doi.org/10.3389/fchem.2020.00212

[49]    T. Khuroo, E.M. Mohamed, S. Dharani, C. Kayalar, T. Ozkan, M.A. Kuttolamadom, Z. Rahman, M.A. Khan. Very-Rapidly Dissolving Printlets of Isoniazid Manufactured by SLS 3D Printing: In Vitro and In Vivo Characterization. *Molecular Pharmaceutics* **19** (2022) 2937-2949. https://doi.org/10.1021/acs.molpharmaceut.2c00306